PHYSICAL REVIEW D **91,** 124058 (2015)

Nonlinear effects for a cylindrical gravitational two-soliton

Shinya Tomizawa[1,*] and Takashi Mishima[2,†]

[1]*Department of Liberal Arts, Tokyo University of Technology, 5-23-22, Nishikamata, Otaku, Tokyo 144-8535, Japan*

[2]*Laboratory of Physics, College of Science and Technology, Nihon University, Narashinodai, Funabashi, Chiba 274-8501, Japan*

(Received 25 February 2015; published 19 June 2015)

Using a cylindrical soliton solution to the four-dimensional vacuum Einstein equation, we study the nonlinear effects of gravitational waves, such as Faraday rotation and the time-shift phenomenon. In a previous work, we analyzed the single-soliton solution constructed using Pomeransky's improved inverse scattering method. In this work, we construct a new two-soliton solution with complex-conjugate poles, by which we can avoid the light-cone singularities that are unavoidable in a single-soliton case. In particular, we compute the amplitudes of nonlinear gravitational waves and the time dependence of the polarizations. Furthermore, we consider the time-shift phenomenon for soliton waves, which means that a wave packet can propagate at a velocity slower than light.

DOI: 10.1103/PhysRevD.91.124058 PACS numbers: 04.70.Bw

I. INTRODUCTION

Many gravitational solitons in general relativity—which describe gravitational solitonic waves propagating throughout spacetime—have been found within the framework of the so-called inverse scattering method [1,2]. In particular, it has attracted a lot of relativists since it can generate black hole solutions in an axisymmetric and stationary case, in addition to exact solutions describing nonlinear gravitational waves on various physical backgrounds. The method was immediately generalized to the higher-dimensional Einstein equations (see the references in Ref. [2]), but such a simple generalization to higher dimensions tends to lead to singular solutions. However, ten years ago Pomeransky [3] succeeded in modifying the original inverse scattering method [4] so that it can generate regular solutions even in higher dimensions. Thanks to this, several black holes solutions were found in five dimensions [5,6].

A diagonal metric form of a cylindrically symmetric spacetime gives the vacuum Einstein equation the extremely simple structure of a linear wave equation in a flat background. An Einstein-Rosen wave—which can be interpreted as a superposition of cylindrical gravitational waves with a $+$ mode only—was obtained as the solution of such an equation [1,7]. However, the existence of nontrivial nondiagonal components of a metric drastically changes the structure of the Einstein equation since it generally yields a $\times$ mode together with nonlinearity. Piran *et al.* [8] numerically studied the nonlinear interaction of cylindrical gravitational waves of both polarization modes and showed that a $+$ mode converts to a $\times$ mode. This phenomenon is called the *gravitational Faraday effect* after the Faraday effect in electrodynamics. Tomimatsu [9] studied the gravitational Faraday rotation for cylindrical gravitational solitons generated by the inverse scattering technique. Moreover, the interaction of gravitational soliton waves with a cosmic string was also studied in Refs. [10–12]. As one of many new attempts to understand strong gravitational effects, we have recently constructed a new cylindrically symmetric single-soliton solution from a Minkowski seed using Pomeransky's inverse scattering method and clarified the behavior of the new solution including the effect similar to the gravitational Faraday rotation.

To further this investigation, in this paper we first construct more complicated gravitational two-soliton solutions with complex-conjugate poles using Pomeransky's method, which are considered as cylindrically symmetric gravitational waves with a rich structure and can be used to study gravitational nonlinear effects. One of the important and remarkable features of the solutions is that there are no null singularities, which generally appear in the case of single-soliton solutions. We may therefore adopt a picture similar to the scattering theory that from the past null infinity one gravitational wave packet comes into "the interaction region" near the symmetric axis and after reflection leaves the region for the future null infinity. The behavior of the wave packet can be analyzed by following the time-sequential images and also by comparing the physical quantities measured in the past and future infinities. As an interesting example, a change of polarization of two independent modes will be treated with both methods.

In the next section, we present the Kompaneets-Jordan-Ehlers form [13] in the most general cylindrical symmetric spacetime and the useful quantities (amplitudes and polarization angles) for the analysis of nonlinear cylindrical

*tomizawasny@stf.teu.ac.jp
†tmishima@phys.ge.cst.nihon-u.ac.jp

gravitational waves, which were first introduced by Piran *et al.* [8] and Tomimatsu [9]. In Sec. III, using the inverse scattering method improved by Pomeransky [3], we generate a two-soliton solution with complex-conjugate poles from Minkowski spacetime. In Sec. IV, we analyze the obtained two-soliton solution by computing the amplitudes and polarization angles for ingoing and outgoing waves. In this section, in particular, by seeing the time dependence of polarizations, we study the gravitational Faraday effect. Furthermore, we mention the difference with the single-soliton solution in our previous paper, and moreover clarify the difference with Tomimatsu's two-soliton solution [9] generated with the Belinsky-Zakharov procedure. In Sec. V, we devote ourselves to a summary and discussion of our results.

II. FORMULAS

We assume that a four-dimensional spacetime admits cylindrical symmetry, namely, that there are two commuting Killing vector fields, an axisymmetric Killing vector $\partial/\partial\phi$, and a spatially translational Killing vector $\partial/\partial z$, where the polar angle coordinate ϕ and the coordinate z have the ranges $0 \le \phi < 2\pi$ and $-\infty < z < \infty$, respectively. Under these symmetry assumptions, the most general metric can be described by the Kompaneets-Jordan-Ehlers form:

$$ds^2 = e^{2\psi}(dz + \omega d\phi)^2 + \rho^2 e^{-2\psi} d\phi^2 + e^{2(\gamma-\psi)}(d\rho^2 - dt^2), \tag{1}$$

where the functions ψ, ω, and γ depend on the time coordinate t and radial coordinate ρ only. Following Refs. [8,9], we introduce the amplitudes

$$A_+ = 2\psi_{,v}, \tag{2}$$

$$B_+ = 2\psi_{,u}, \tag{3}$$

$$A_\times = \frac{e^{2\psi}\omega_{,v}}{\rho}, \tag{4}$$

$$B_\times = \frac{e^{2\psi}\omega_{,u}}{\rho}, \tag{5}$$

where the advanced ingoing and outgoing null coordinates u and v are defined by $u = (t-\rho)/2$ and $v = (t+\rho)/2$, respectively. The indices $+$ and $\times$ denote the quantities associated with the respective polarizations. Then, the vacuum Einstein equation can be written in terms of these quantities; actually, the nonlinear differential equations for the functions ψ and ω are replaced by

$$A_{+,u} = \frac{A_+ - B_+}{2\rho} + A_\times B_\times, \tag{6}$$

$$B_{+,v} = \frac{A_+ - B_+}{2\rho} + A_\times B_\times, \tag{7}$$

$$A_{\times,u} = \frac{A_\times + B_\times}{2\rho} - A_+ B_\times, \tag{8}$$

$$B_{\times,v} = -\frac{A_\times + B_\times}{2\rho} + A_\times B_+, \tag{9}$$

and the function γ is determined by

$$\gamma_{,\rho} = \frac{\rho}{8}(A_+^2 + B_+^2 + A_\times^2 + B_\times^2), \tag{10}$$

$$\gamma_{,t} = \frac{\rho}{8}(A_+^2 - B_+^2 + A_\times^2 - B_\times^2). \tag{11}$$

The ingoing and outgoing amplitudes are, respectively, defined by

$$A = \sqrt{A_+^2 + A_\times^2}, \qquad B = \sqrt{B_+^2 + B_\times^2}, \tag{12}$$

and the polarization angles θ_A and θ_B for the respective wave amplitudes are given by

$$\tan 2\theta_A = \frac{A_\times}{A_+}, \qquad \tan 2\theta_B = \frac{B_\times}{B_+}. \tag{13}$$

III. TWO-SOLITON SOLUTION

In this work, as a seed, we consider Minkowski spacetime written in cylindrical coordinates whose 2×2 part of the metric $g_0 \coloneqq (g_{0ab})(a, b = z, \phi)$ and metric function $f_0 \coloneqq e^{2(\gamma_0 - \psi_0)}$ are given by, respectively,

$$g_0 = \mathrm{diag}(1, \rho^2), \qquad f_0 = 1. \tag{14}$$

Following the inverse scattering method which Pomeransky improved [3], we construct a two-soliton solution with complex-conjugate poles. First, we remove the trivial solitons with (1,0) at $t = a_1$ and $t = a_2$ ($\bar{a}_2 = a_1$) from the seed metric, and then we obtain the metric

$$g_0{}' = \mathrm{diag}\left(\frac{|\mu_1|^4}{\rho^4}, \rho^2\right) = (|w|^4, \rho^2), \tag{15}$$

where $w \coloneqq \mu_1/\rho[\mu_1 = \bar{\mu}_2 = \sqrt{(t-a_1)^2 - \rho^2} - (t - a_1)]$. Note that a_1 is a complex parameter and the bar denotes complex conjugation. Next, we reintroduce the nontrivial solitons with $(1, a)$ and $(1, \bar{a})$. Then we obtain the two-soliton solution as

$$g_{ab} = (g'_0)_{ab} - \sum_{k,l=1}^{2} \frac{(g'_0)_{ac} m_c^{(k)} (\Gamma^{-1})_{kl} m_d^{(l)} (g'_0)_{db}}{\mu_k \mu_l}, \quad (16)$$

$$f = f_0 \frac{\det(\Gamma_{kl})}{\det(\Gamma_{kl}(c=0))}, \quad (17)$$

where

$$\Gamma_{kl} = \frac{m_a^{(k)} (g'_0)_{ab} m_b^{(l)}}{-\rho^2 + \mu_k \mu_l}, \quad (18)$$

$$m_a^{(k)} = m_{0b}^{(k)} (\Psi_0^{-1}(\rho, t, \mu_k))_{ba}. \quad (19)$$

$\Psi_0(\rho, t, \lambda)$ is a generating matrix for the seed g'_0, which is given by

$$\Psi_0(\rho, t, \lambda) = \mathrm{diag}\left(\frac{(\rho^2 + 2t\lambda + \lambda^2)^2}{(\tilde{\mu}_1 - \lambda)^2 (\tilde{\mu}_2 - \lambda)^2}, \rho^2 + 2t\lambda + \lambda^2 \right), \quad (20)$$

where $\tilde{\mu}_k = \rho^2/\mu_k (k = 1, 2)$.

We present the metric in the Kompaneets-Jordan-Ehlers form [13], which describes the most general cylindrically symmetric spacetime,

$$ds^2 = e^{2\psi}(dz + \omega d\phi)^2 + \rho^2 e^{-2\psi} d\phi^2 + e^{2(\gamma - \psi)}(d\rho^2 - dt^2), \quad (21)$$

where the functions ψ, ω, and γ depend on the time coordinate t and radial coordinate ρ only, and they are explicitly given by

$$e^{2\psi} = |w|^4 \left(1 - \frac{\mathcal{A}}{\mathcal{B}} \right), \quad (22)$$

$$\omega = -\frac{(|w|^2 - 1)^2}{\rho} \frac{\mathcal{C}}{\mathcal{B} - \mathcal{A}}, \quad (23)$$

$$e^{2\gamma} = \frac{|w|^4 (\mathcal{B} - \mathcal{A})}{(w - \bar{w})^2 |w^2 - 1|^6 (|w|^2 - 1)^6}, \quad (24)$$

with

$$\mathcal{A} = 2\Re\left[\frac{(|w|^2 - 1)^4 (\bar{w}^2 - 1)^4}{\bar{w}^2 (w^2 - 1)} (X^2 + c^2 Y^2) \right] - 2 \frac{(|w|^2 - 1)^3 |w^2 - 1|^4}{|w|^2} (|X|^2 + |c|^2 |Y|^2), \quad (25)$$

$$\mathcal{B} = \frac{1}{|w^2 - 1|^2} |X^2 + c^2 Y^2|^2 - \frac{1}{(|w|^2 - 1)^2} (|X|^2 + |c|^2 |Y|^2)^2, \quad (26)$$

$$\mathcal{C} = 2\Re\left[\frac{\bar{c}(\bar{w}^2 - 1)^2}{\bar{w}(w^2 - 1)} (X^2 + c^2 Y^2) \right] - 2\Re\left[\frac{\bar{c}(w^2 - 1)^2}{w(|w|^2 - 1)} \right] (|X|^2 + |c|^2 |Y|^2), \quad (27)$$

$$X = (w^2 - 1)^2 (|w|^2 - 1)^2, \quad (28)$$

$$Y = \frac{|w|^2 w}{\rho^2}, \quad (29)$$

$$c = 2aa_1. \quad (30)$$

Here, $\Re[]$ denotes a real part of [].

After using the time-translational invariance of the system to rewrite the parameter a_1 as iq (i is $\sqrt{-1}$ and q is a positive number), we can simplify the metric by introducing the following new coordinates (x, y):

$$t = qxy, \qquad \rho = q\sqrt{(x^2 + 1)(y^2 - 1)}. \quad (31)$$

Note that

$$\mu_1 = \bar{\mu}_2 = q(x + i)(1 - y). \quad (32)$$

Let us put $a = a_r + a_i i (a_r, a_i \in \boldsymbol{R})$. In the coordinate system (x, y), the metric can be written as

$$ds^2 = \frac{\mathcal{Y}}{\mathcal{X}} \left(dz + \frac{\mathcal{Z}}{\mathcal{Y}} d\phi \right)^2 + \rho^2 \frac{\mathcal{X}}{\mathcal{Y}} d\phi^2 + \frac{\mathcal{X}}{4096 q^4 (x^2 + y^2)^5} \left(-\frac{dx^2}{x^2 + 1} + \frac{dy^2}{y^2 - 1} \right), \quad (33)$$

where the metric functions $\mathcal{X}, \mathcal{Y}$, and $\mathcal{Z}$ are

$$\begin{aligned}
\mathcal{X} &= a_i^4(y-1)^2(y+1)^6 + 2a_i^2(y+1)^2(a_r^2(y-1)^2(y+1)^4 + 64q^2(x^4(y(9y-8)+1) + 2x^2(y(y+4)-3)y^2 + y^6 + y^4)) \\
&\quad - 512a_i a_r q^2 x(y+1)^2(x^2-(y-2)y)(x^2(2y-1)+y^2) + a_r^4(y-1)^2(y+1)^6 \\
&\quad + 128a_r^2q^2(y+1)^2(2x^6 + x^4((8-3y)y-1) + 2x^2y^2(2(y-2)y+3) + y^6 - y^4) + 4096q^4(x^2+y^2)^4, \\
\mathcal{Y} &= a_i^4(y^2-1)^4 + 2a_i^2(y^2-1)(a_r^2(y^2-1)^3 + 64q^2(x^4(9y^2-1) + 2x^2(y^2+3)y^2 + y^6 - y^4)) \\
&\quad - 1024a_i a_r q^2 x(x^2+1)y(y^2-1)(x-y)(x+y) + a_r^4(y^2-1)^4 \\
&\quad + 128a_r^2q^2(y^2-1)(2x^6 + x^4 + (4x^2+1)y^4 - 3(x^2+2)x^2y^2 + y^6) + 4096q^4(x^2+y^2)^4, \\
\mathcal{Z} &= -32q^2(y+1)(a_i^3x(y-1)(y+1)^3(x^2(1-3y)+(y-3)y^2) + a_i^2a_r(y-1)(y+1)^3(x^4 - 3x^2(y-1)y - y^3) \\
&\quad + a_i x(y-1)(a_r^2(y+1)^3(x^2(1-3y)+(y-3)y^2) + 64q^2(x^2+y^2)^3) \\
&\quad + a_r(a_r^2(y-1)(y+1)^3(x^4 - 3x^2(y-1)y - y^3) - 64q^2(x^2+y)(x^2+y^2)^3).
\end{aligned}$$

IV. ANALYSIS

Let us investigate how the new gravitational solitonic waves propagate throughout spacetime from several viewpoints. For the convenience of explanation, we introduce the modulus k and the angle θ of the complex parameter a,

$$k = |a|, \qquad \theta = \mathrm{Arg}(a).$$

In the following analysis, we only consider the case $q = 1$, because the parameter q can be normalized by a scaling of the coordinates.

First we briefly show the qualitative behavior of the waves near the axis. The panels $n = 0, \ldots, 7$ in Fig. 1 show the various behaviors of the total amplitude ($A_{\mathrm{tot}} = \sqrt{A^2 + B^2}$) from the spacetime viewpoint. The figures are plotted in the ranges $-5 \le t \le 5$ and $0 \le \rho \le 5$ under the parameter setting $q = 1$, $k = 2$, and $\theta = n\pi/4 (n = 0 \sim 7)$. Some of the behaviors are also displayed in Fig. 2 by superimposing the instantaneous graphs that correspond to $t = 0$ and $t = \pm n, (n = 1 \sim 3)$, respectively. From the behaviors of the amplitudes we may consider the gravitational solitonic waves to be regular wave packets, which first come into the region near the symmetric axis from past null infinity, and leave the axis after reflection for future null infinity. On first inspection, the various complex behaviors seem to be generated by a certain kind of nonlinear effect near the axis. For example, in Figs. 1 and 2, at the angle $\theta = \pi/4$ the initial two wave packets coalesce into one packet, while at the angle $\theta = 3\pi/4$ the initial single wave packet splits in two. These remarkable phenomena seem to occur very close to the axis, so that we may say that the neighborhood around the axis is the region where nonlinear effects become strong.

In the subsequent subsections, we will see the detailed behavior of the waves propagating near the boundaries of spacetime, particularly focusing on nonlinear effects.

A. Initial amplitudes

We now look at the initial amplitudes for the ingoing and outgoing waves. At the initial time $t = 0$, we have the ingoing and outgoing wave amplitudes

$$A = \frac{4q}{\sqrt{\rho^2+q^2}}\sqrt{\frac{N + 128a_i a_r q^3(\rho^2+q^2)\rho}{D}}, \tag{34}$$

$$B = \frac{4q}{\sqrt{\rho^2+q^2}}\sqrt{\frac{N - 128a_i a_r q^3(\rho^2+q^2)\rho}{D}}, \tag{35}$$

where

$$\begin{aligned}
N &:= (|a|^4 + 64a_i^2q^2)\rho^6 + 64q^4(|a|^2 + a_i^2)\rho^4 \\
&\quad + 64q^6(|a|^2 + a_r^2)\rho^2 + 64q^8a_r^2, \\
D &:= (|a|^2 + 64q^2)^2\rho^8 + 256q^4(|a|^2 + a_r^2 + 64q^2)\rho^6 \\
&\quad + 128q^6(|a|^2 + 4a_r^2A_{\mathrm{tot}} + 192q^2)\rho^4 \\
&\quad + 256q^8(a_r^2 + 64q^2)\rho^2 + 4096q^{12}.
\end{aligned}$$

As is shown in Fig. 2, the disturbances for the total amplitude A_{tot}, which is related to the C-energy density, is localized in the neighborhood of the axis.

B. Asymptotic behaviors

1. Timelike infinity

Next we consider the asymptotic behaviors of the waves at late time $t \to \infty$. At $t \to \infty$, the metric behaves as

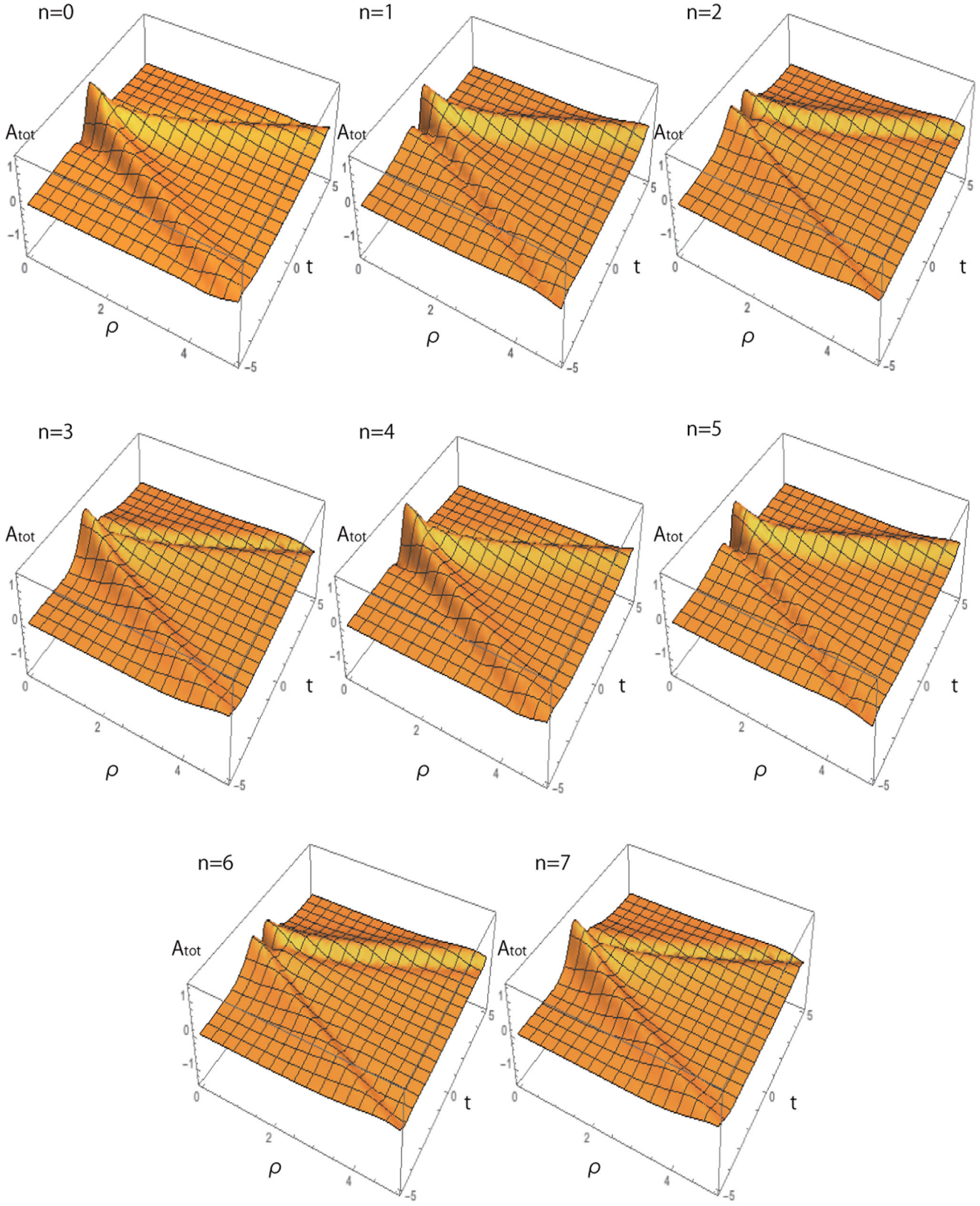

FIG. 1 (color online). The total amplitude $A_{\mathrm{tot}} = \sqrt{A^2 + B^2}$ in the (ρ, t) plane for $(k, \theta) = (2, n\pi/4)(n = 0, 1, \ldots, 7)$.

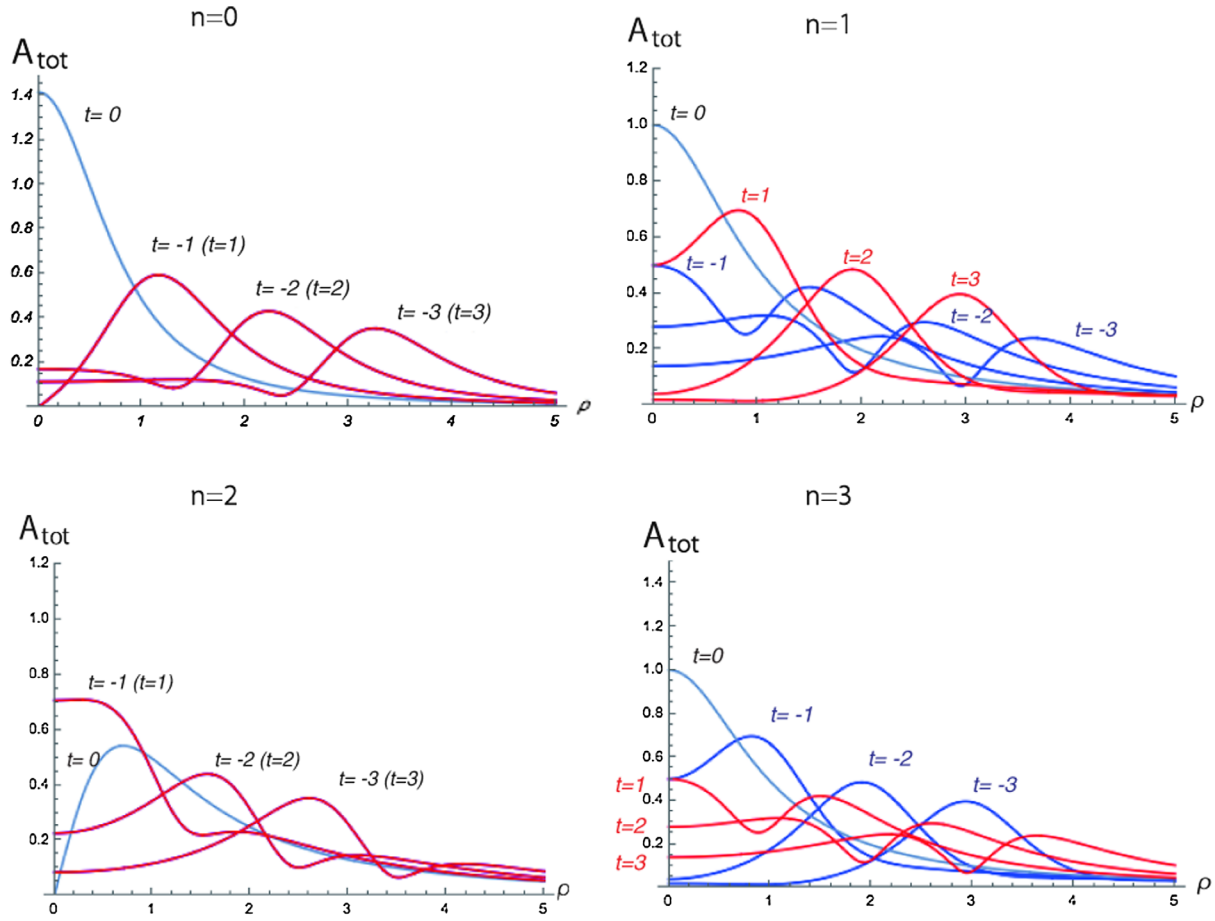

FIG. 2 (color online). Time dependence of the total amplitude A_{tot} for $(k,\theta,q)=(2,n\pi/4,1)(n=0,1,2,3)$. The blue and red curves denote incident waves and reflected waves, respectively, for $t=,\pm1,\pm2,\pm3$. The violet curves in the case $n=0,2$ show that the incident and reflected waves entirely overlap.

$$ds^2 \simeq \left(1-\frac{a_r^2}{4t^2}\right)\left[dz+a_r\left(1+\frac{\rho^2}{4t^2}\right)d\phi\right]^2+\rho^2\left(1+\frac{a_r^2}{4t^2}\right)d\phi^2+\left(1+\frac{a_r^2}{4t^2}\right)(-dt^2+d\rho^2). \tag{36}$$

Here let us introduce the new coordinate $\tilde{z}:=z+a_r\phi$, so that $\partial/\partial\tilde{z}$ is also a translationally symmetric Killing vector; then, we can show that this asymptotic metric is that of Minkowski spacetime. Therefore, both ingoing and outgoing waves vanish at late time. We have the asymptotic amplitudes

$$A \simeq B \simeq \frac{a_r}{2t^2}+\mathcal{O}(t^{-3}). \tag{37}$$

In particular, for $a_r=0$, the amplitudes behave in a different way,

$$A \simeq B \simeq \frac{a_i q}{t^3}+\mathcal{O}(t^{-4}). \tag{38}$$

In this region, the polarization angles θ_A and θ_B for outgoing and ingoing waves behave as

$$\tan\theta_A \simeq \tan\theta_B \simeq 1. \tag{39}$$

This shows that, regardless of the values of the parameters, the $\times$ mode becomes dominant at late time.

2. Spacelike infinity

Let us consider gravitational waves near spacelike infinity $\rho\to\infty$. In the limit of $\rho\to\infty$, we have the following asymptotic metric form:

$$ds^2 \simeq \left(1-\frac{4|a|^2q}{(|a|^2+64q^2)\rho}\right)\left[dz+\frac{32a_rq^2}{|q|^2+64q^2}d\phi\right]^2+\rho^2\left(1+\frac{4|a|^2q}{(|a|^2+64q^2)\rho}\right)d\phi^2+\frac{(|a|^2+64q^2)^2}{4096q^4}(-dt^2+d\rho^2). \tag{40}$$

If we use the new coordinate

$$\tilde{z} = z + \frac{32 a_r q^2}{(|a|^2 + 64q^2)}\phi, \tag{41}$$

we immediately find that this spacetime is Minkowski spacetime with the deficit angle

$$D = 2\pi \frac{|a|^2}{|a|^2 + 64q^2}. \tag{42}$$

The wave amplitudes behave as

$$A \simeq B \simeq \frac{\sqrt{|a|^4 + 64 a_i^2 q^2}}{(|a|^2 + 64q^2)\rho^2} + \mathcal{O}(\rho^{-3}). \tag{43}$$

For $a_i \neq 0$, the polarization angles approach the values

$$\tan\theta_A \simeq -\tan\theta_B \simeq \frac{|a|^2 - \sqrt{|a|^4 + 16 a_i^2 q^2}}{16 a_i q}, \tag{44}$$

and for $a_i = 0$, they behave as

$$\tan\theta_A \simeq \tan\theta_B \simeq 0. \tag{45}$$

3. Axis

Now we look at the behavior of the waves on the axis of symmetry $\rho = 0$. Near the axis, the metric behaves as

$$\begin{aligned} ds^2 \simeq{}& \frac{4(q^2+t^2)^2}{4(t^2+q^2)^2 + (t a_r - q a_i)^2}(dz + a_r d\phi)^2 \\ &+ \frac{4(t^2+q^2)^2 + (t a_r - q a_i)^2}{4(q^2+t^2)^2}\rho^2 d\phi^2 \\ &+ \frac{4(t^2+q^2)^2 + (t a_r - q a_i)^2}{4(q^2+t^2)^2}(-dt^2 + d\rho^2). \end{aligned} \tag{46}$$

Using the coordinate $\tilde{z} = z + a_r\phi$, we have the metric

$$\begin{aligned} ds^2 \simeq{}& \frac{4(q^2+t^2)^2}{4(t^2+q^2)^2 + (t a_r - q a_i)^2} d\tilde{z}^2 \\ &+ \frac{4(t^2+q^2)^2 + (t a_r - q a_i)^2}{4(q^2+t^2)^2}\rho^2 d\phi^2 \\ &+ \frac{4(t^2+q^2)^2 + (t a_r - q a_i)^2}{4(q^2+t^2)^2}(-dt^2 + d\rho^2). \end{aligned} \tag{47}$$

It is straightforward to show that the ratio of the length of the circumference to the radial distance on the axis is

$$\lim_{\rho\to 0} \frac{\int_0^{2\pi}\sqrt{g_{\phi\phi}}d\phi}{\int_0^{\rho}\sqrt{g_{\rho\rho}}d\rho} = 2\pi. \tag{48}$$

This equation means that no deficit angle is present on the axis, which is in contrast to spacelike infinity. In the limit of $\rho \to 0$, the wave amplitudes behave as

$$A \simeq B \simeq \frac{|a_r t^2 - 2 a_i q t - a_r q^2|\sqrt{16(t^2+q^2)^2(a_i q - a_r t)^2 + \{(a_r t - a_i q)^2 - 4(t^2+q^2)^2\}^2}}{2(t^2+q^2)^2[(a_r t - a_i q)^2 + 4(q^2+t^2)^2]}. \tag{49}$$

The polarizations are

$$\tan 2\theta_A \simeq \tan 2\theta_B \simeq -\frac{(2t^2 + 2q^2 - a_r t + a_i q)(2t^2 + 2q^2 + a_r t - a_i q)}{4(t^2+q^2)(a_i q - a_r t)}. \tag{50}$$

4. Null infinity

At null infinity $v \to \infty$, the wave amplitudes behave as

$$A \simeq 2 p_1 \sqrt{\frac{N_1}{D_1 v^3}}, \tag{51}$$

$$B \simeq \frac{8 p_1^3}{p_1^4 + q^2}\sqrt{\frac{N_2}{D_2 v}}, \tag{52}$$

where

$$N_1 = (|a|^4 q^4 + 64 a_i^2 q^6) - 128 a_r a_i q p_1^2 (q^2 + p_1^4)^2 + 64(|a|^2 + a_i^2) q^4 p_1^4 + 64(|a|^2 + a_r^2) q^2 p_1^8 + 64 a_r^2 p_1^{12}, \tag{53}$$

$$D_1 = q^4(|a|^2+64q^2)^2+256q^4(|a|^2+a_r^2+64q^2)p_1^4+1024a_ra_iqp_1^6(q^2-p_1^4)+384q^2(3|a|^2-4a_r^2+64q^2)p_1^8 + 256(a_r^2+64q^2)p_1^{12}+4096p_1^{16}, \tag{54}$$

$$N_2 = |a|^4q^4+64a_i^2q^6-384a_ra_ip_1^2q(q^4+p_1^8)+192q^2p_1^4(|a|^2-5a_i^2)(q^2-p_1^4)+1280a_ra_iq^3p_1^6+64a_r^2p_1^{12}, \tag{55}$$

$$D_2 = q^4(|a|^2+64q^2)^2+256q^4(|a|^2+a_r^2+64q^2)p_1^4+1024a_ra_iqp_1^6(q^2-p_1^4)+384q^2(3|a|^2-4a_r^2+64q^2)p_1^8 + 256(a_r^2+64q^2)p_1^{12}+4096p_1^{16}, \tag{56}$$

and $p_1 = \sqrt{2u+\sqrt{4u^2+q^2}}$.

C. Faraday effect

In this subsection, using the two-soliton solution, we study the gravitational Faraday effect, which is a phenomenon in which an outgoing (ingoing) wave amplitude corresponding to the + mode converts to an outgoing (ingoing) wave amplitude corresponding to the × mode due to the interaction with an ingoing (outgoing) wave with the × mode. Let us see how the + modes convert to the × modes while the corresponding gravitational waves are propagating along null rays from the axis $\rho = 0$ to null infinity $v \to \infty$. It is most interesting to analyze it in the cases when $a_r^2 - 16q^2 - 8a_iq > 0$ and $a_r^2 - 16q^2 + 8a_iq > 0$, since both polarization angles θ_A and θ_B completely vanish on the axis four times, i.e., at $t = t_{\pm\pm}$, where $t_{\pm\pm}$ are defined by, respectively,

$$t_{+\pm} = \frac{a_r \pm \sqrt{a_r^2-16q^2-8a_iq}}{4}, \tag{57}$$

$$t_{-\pm} = \frac{-a_r \pm \sqrt{a_r^2-16q^2+8a_iq}}{4}. \tag{58}$$

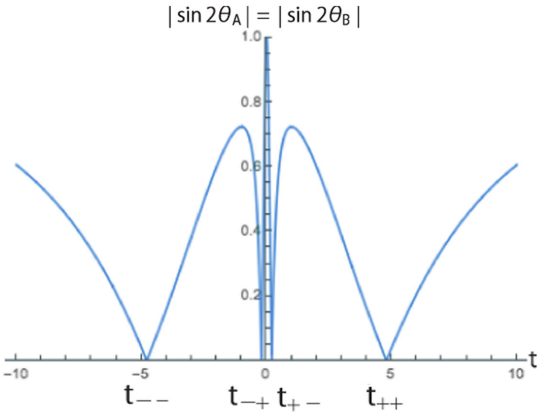

FIG. 3 (color online). The behaviors of $|\sin 2\theta_A|$ and $|\sin 2\theta_B|$ for $(a_r, a_i, q) = (10, 0, 1)$ on the axis.

As shown in Fig. 3, θ_A and θ_B have time dependence on $\rho = 0$ and the × mode vanishes there at $t = {}_{\pm\pm}$.

The upper-left graph in Fig. 4 shows that the pure + mode wave passing $(t, \rho) = (t_{++}, 0)$ partially converts to the × mode wave and that its conversion comes to a stop asymptotically at $v \to \infty$. The ratio of the × mode to the + mode monotonously approaches a certain constant value. In this process, a complete conversion of + to ×, or of × to + does not occur. The upper-right graph in Fig. 4 illustrates that the pure + gravitational wave passing $(t, \rho) = (t_{+-}, 0)$ converts a little to the × mode and soon converts to the pure + mode. After that, a small conversion occurs and again becomes the pure + mode twice and θ_B approaches a nonzero value. Finally, its conversion comes to a stop asymptotically at $v \to \infty$. The ratio of the × mode to the + mode becomes a certain constant value. The lower-left graph in Fig. 4 shows that the pure + gravitational wave passing $(t, \rho) = (t_{-+}, 0)$ completely converts to the × mode, and afterwards partially converts to the + mode. At $v \to \infty$, the × mode becomes dominant. The lower-right graph in Fig. 4 illustrates that the pure + gravitational wave passing $(t, \rho) = (t_{--}, 0)$ partially converts to the × mode. At $v \to \infty$, θ_B asymptotically approaches a certain constant.

Finally, let us consider the gravitational wave passing $(t, \rho) = (t_\times, 0)$, where $t_\times = a_iq/a_r$, when no + mode is present at the axis. As shown in Fig. 5, the pure × mode partially converts to the + mode, but the × mode again increases, and at $v \to \infty$ the value of θ_B becomes a constant.

D. Time shift

No we investigate the time-shift phenomenon as a nonlinear effect, which means that a wave packet propagates at a velocity slower than light. Following the analysis in Ref. [14], where a procedure for measuring a time shift for gravitational solitons was proposed, we numerically analyze the asymptotic behavior of the wave packets at future null infinity $v \to \infty$ and past null infinity $u \to -\infty$. In principle, we can find a time shift of the wave

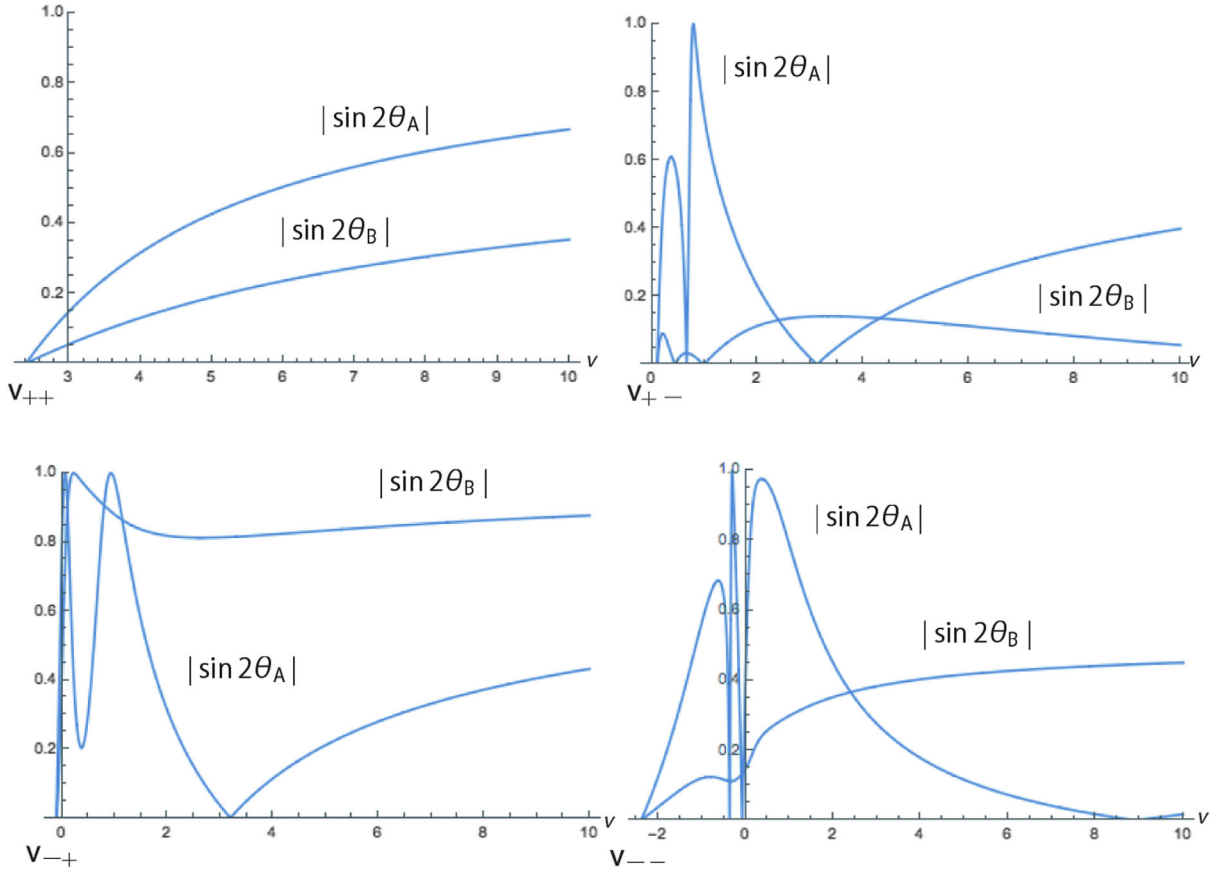

FIG. 4 (color online). $|\sin 2\theta_A|$ and $|\sin 2\theta_B|$ along the outgoing null rays u_{++}, u_{+-}, u_{-+},u_{--} for $(a_r, a_i, q) = (10, 0, 1)$.

amplitudes by comparing its arrival time at future null infinity with that of a massless test particle starting at past null infinity at the same time. As illustrated in Fig. 6, an incoming massless particle propagating along $v = 0$ from past null infinity $u = -\infty$ arrives at the axis $\rho = 0$, and after reflection it propagates along $u = 0$ toward future null infinity $v = \infty$. Let us see how slow a wave packet with a peak near $u = 0$ and $v = 0$ is, compared with the massless particle.

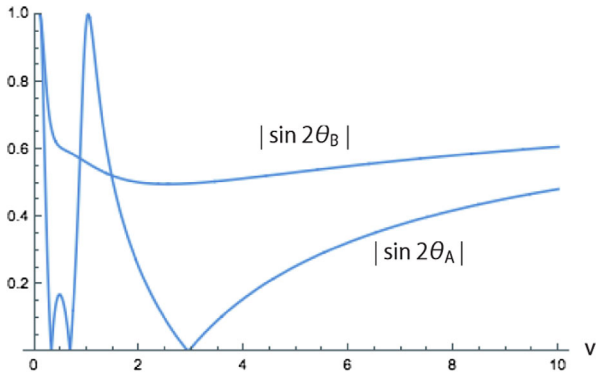

FIG. 5 (color online). $|\sin 2\theta_A|$ and $|\sin 2\theta_B|$ along the outgoing null ray $u_\times$ for $(a_r, a_i, q) = (10, 2, 1)$.

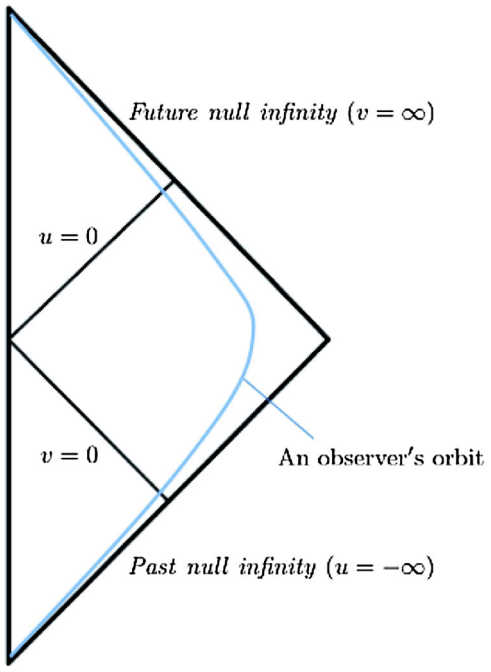

FIG. 6 (color online). The orbit of a massless particle propagating in an incoming radial direction along $v = 0$, reflecting at the axis $\rho = 0$, and propagating in an outgoing direction along $u = 0$.

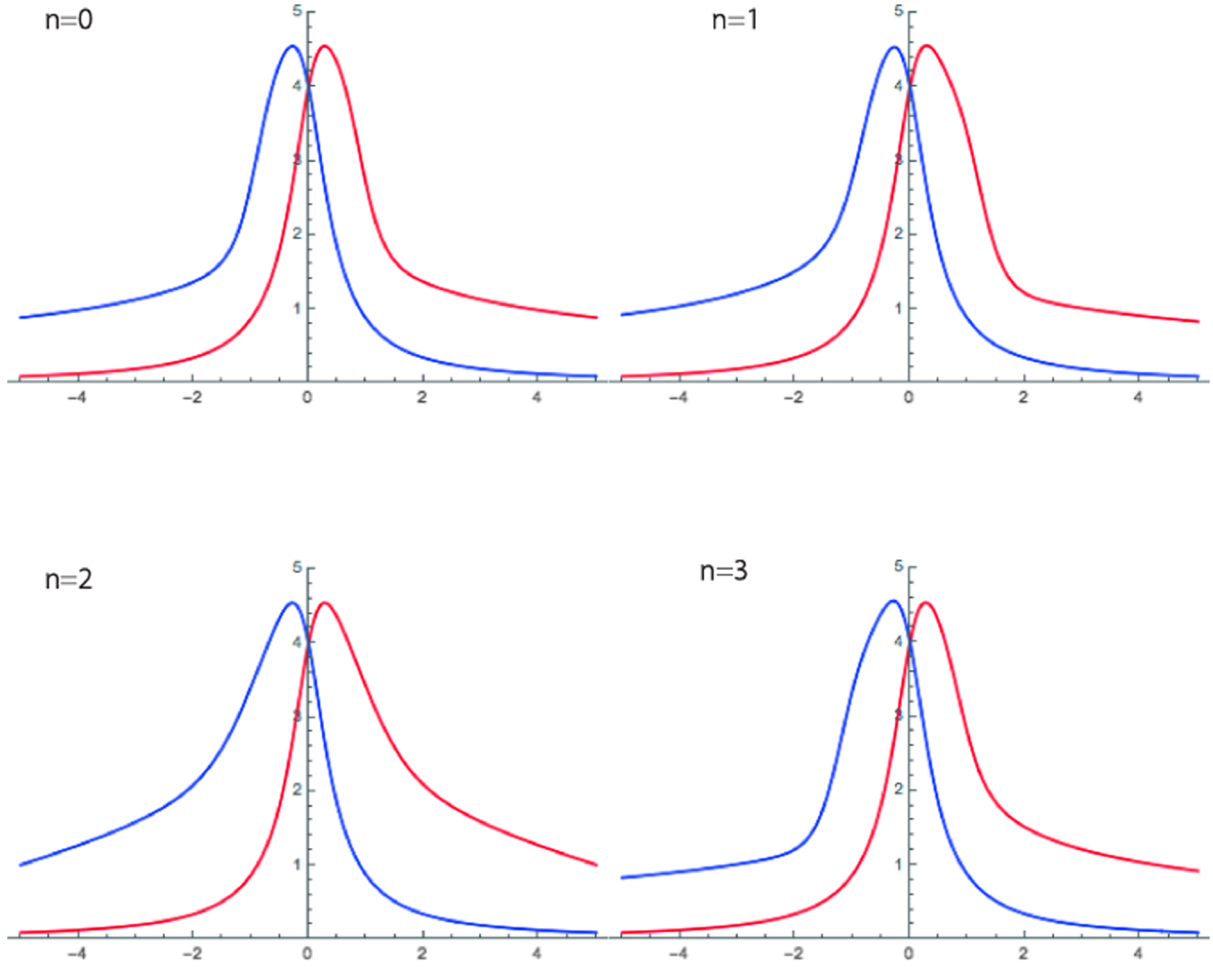

FIG. 7 (color online). Time shift for $(k, \theta, q) = (1000, n\pi/4, 1)(n = 0, 1, 2, 3)$. The blue and red curves show the incident waves at past null infinity and the reflected waves at future null infinity, respectively.

In Fig. 7, the blue curves denote the amplitudes for ingoing waves near past null infinity, $\lim_{u\to-\infty} A\sqrt{-u}$, and the red curves denote the amplitudes for outgoing waves near future null infinity, $\lim_{v\to\infty} B\sqrt{v}$, for $(k, \theta) = (2, n\pi/4)$ $(n = 0, 1, 2, 3)$, where the amplitudes are multiplied by $(-u)^{\frac{1}{2}}$ and $v^{\frac{1}{2}}$ due to the apparent decay at null infinity. We can interpret these results as follows. Let us consider an incoming massless test particle starting from past null infinity and propagating along a null geodesic $v = 0$. The particle is reflected at the axis $\rho = 0$, and then propagates to future null infinity along a null geodesic $u = 0$. An observer at past null infinity sees an ingoing wave packet earlier than an incoming radial photon, while at future null infinity they see the outgoing wave packet after the outgoing photon. This shows the time-shift phenomenon. Moreover, we would like to comment that for very large values (regardless of the difference between the values of θ), the wave packet always propagates slower than a massless test particle, as seen in Fig. 7. It can neither collide nor split in the process.

E. Collision, coalescence, and the splitting of solitons

Besides the time-shift phenomena, when $k \approx |q|$ the ingoing and outgoing waves take various shapes depending on the phase, as seen in Fig. 8. As seen in these graphs, both the ingoing and outgoing waves can have two peaks.

For $n = 0(\theta = 0)$, there are two ingoing wave packets (one with a small peak and one with a large peak near past null infinity) and two outgoing wave packets (one with a small peak and one with a large peak near future null infinity). This obviously shows that two gravitational solitons collide, which occurs near the axis $\rho \simeq 0$, and then the larger one of the two solitons overtakes the smaller one. For $n = 6(\theta = \pi/2)$, conversely, the smaller one collides with the larger one and then overtakes it.

For $n = 3$ $(\theta = \pi/4)$, there are two ingoing solitons at past null infinity, but a single outgoing soliton at near future null infinity. This shows that two solitons coalesce (in a reflection at the axis). In contrast, as seen for $n = 9$ $(\theta = 3\pi/4)$, a single wave packet splits into two wave packets. Such phenomena do not happen for other

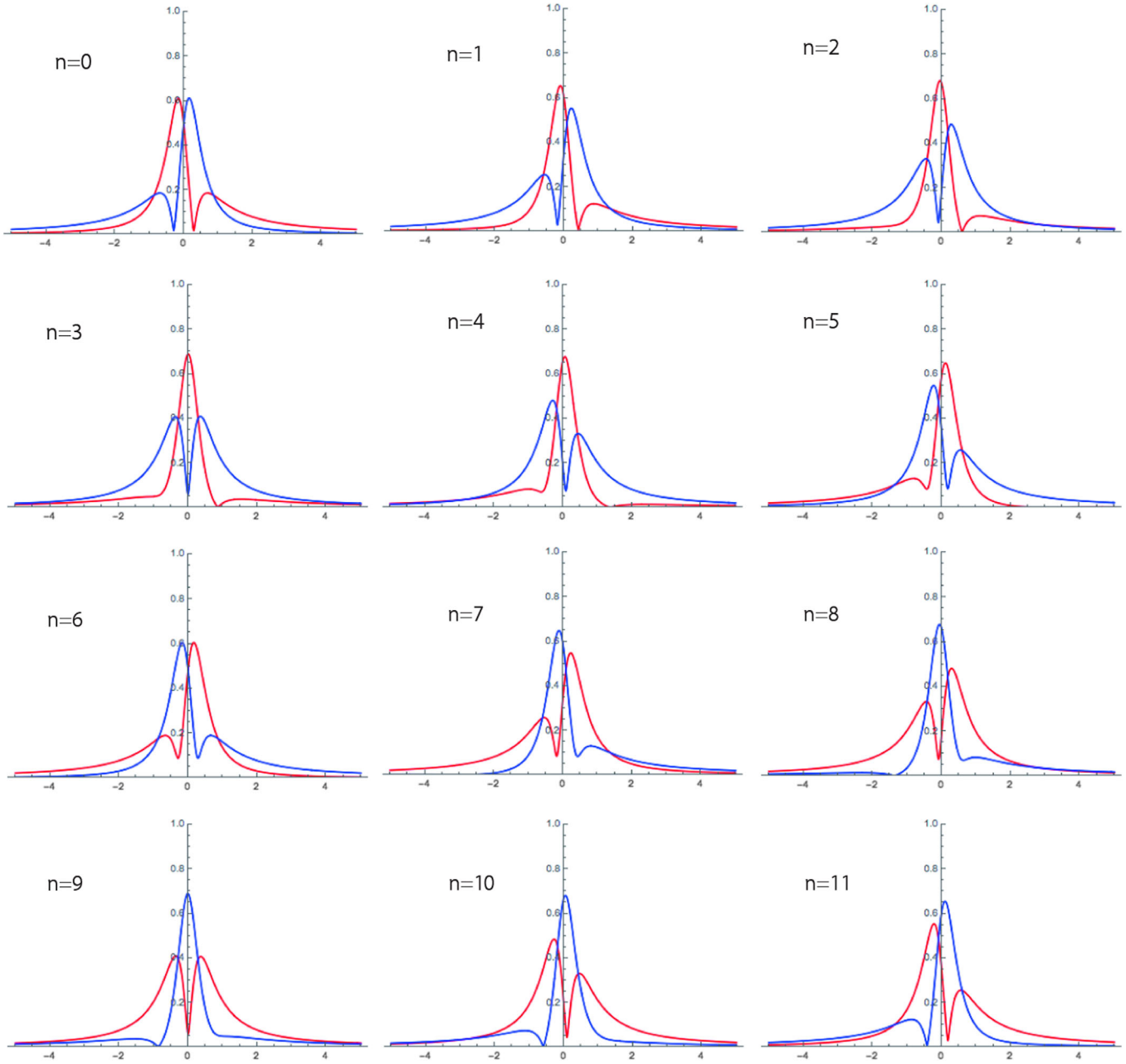

FIG. 8 (color online). Amplitudes of the ingoing and outgoing waves for $(k, \theta, q) = (2, n\pi/12, 1)(n = 0, 1, \ldots, 11)$. The blue and red curvess show the incident waves at past null infinity and reflectional waves at future null infinity, respectively.

solitons, such as solitons of the Korteweg–de Vries (KdV) equation.

V. SUMMARY AND DISCUSSION

In this paper, using Pomeransky's inverse scattering method for a cylindrically symmetric spacetime and starting from the Minkowski seed, we have obtained the two-soliton solution (which has two complex-conjugate poles) to the vacuum Einstein equation with cylindrical symmetry. As with the one-soliton solution with a real pole (in our previous work [15]), it has been numerically shown that the two-soliton solution (presented in this work) describes a gravitational wave packet with two polarizations that comes from past null infinity, is reflected at the axis, and returns to future null infinity. The one-soliton solution in Ref. [15] describes a shock wave pulse with infinite amplitude propagating at the velocity of light, which yields null singularities, but the two-soliton solution is entirely free from such singular behavior. This fact itself should not be surprising because in the previous work [9] a two-soliton solution with complex-conjugate poles and without any singularities was constructed.

In this work, using the two-soliton solution, we have studied the nonlinear effect of cylindrically symmetric gravitational waves, focusing particularly on (i) the gravitational Faraday effect, (ii) the time-shift phenomenon, and (iii) the collision process of two solitons.

(i) The polarization angles θ_A and θ_B of gravitational waves on the axis have a time dependence. In particular, if $a_r^2-16q^2-8a_iq>0$ or $a_r^2-16q^2+8a_iq>0$, at the times $t=t_{\pm\pm}$ the $\times$ mode completely vanishes on the axis $\rho=0$ and only the $+$ mode is present there. In this case, we have studied how the pure $+$ mode on the axis converts to the $\times$ mode while it is propagating along the null rays $u=u_{\pm\pm}$. It was shown that in any case the polarization angles asymptotically approach a certain nonzero constant, which means that both modes are present at future null infinity.

(ii) Here we said that the time shift is a phenomenon wherein a wave packet of a gravitational wave propagates at a velocity slower than light. This is slightly different from the context used in the field of usual soliton theories, where this term (which is also called a phase shift) is used to imply that when two solitonic waves collide, each position shifts compared to when it propagates alone. In the case of cylindrical gravitational solitonic waves, it is evident that this phenomenon is due to the self-interaction of a gravitational wave when an ingoing cylindrical wave reflects, rather than the interaction due to the collision of two solitonic waves, since in a region far from the axis this gravitational soliton seems to propagate at the velocity of light.

(iii) For the two-soliton solution in this paper, we have clarified that two gravitational solitons can coalesce into a single soliton, and also that a single soliton can split into two via the nonlinear effect of gravitational waves. Such phenomena cannot be seen for solitons of other integrable equations such as solitons of the KdV equation. For the KdV equation, when two solitons traveling in the same direction collide (the amplitude is not simply the sum of the two individual solitons), each soon separates from the other and then asymptotically approaches the same wave-pulse shape as before the collision.

ACKNOWLEDGMENTS

This work of S. T. was supported by the Grant-in-Aid for Young Scientists (B) (Number 26800120) from Japan Society for the Promotion of Science (JSPS).

[1] H. Stephani, D. Kramer, M. MacCallum, C. Hoenselaers, and E. Herlt, *Exact solutions of Einstein's Field Equations*, 2nd edition (Cambridge University Press, Cambridge, England, 2003).
[2] V. A. Belinski and E. Verdaguer, *Gravitational Solitons* (Cambridge University Press, Cambridge, England, 2001).
[3] A. A. Pomeransky, Phys. Rev. D **73**, 044004 (2006).
[4] V. A. Belinsky and V. E. Zakharov, Sov. Phys. JETP, **49**, 985 (1979).
[5] H. Iguchi, K. Izumi, and T. Mishima, Prog. Theor. Phys. Suppl. **189**, 93 (2011).
[6] R. Emparan and H. S. Reall, Living Rev. Relativity **11**, 6 (2008).
[7] A. Einstein and N. Rosen, J. Franklin Inst. **223**, 43 (1937).
[8] T. Piran, P. N. Safier, and R. F. Stark, Phys. Rev. D **32**, 3101 (1985).
[9] A. Tomimatsu, Gen. Relativ. Gravit. **21**, 613 (1989).
[10] A. Economou and D. Tsoubelis, Phys. Rev. D **38**, 498 (1988).
[11] B. C. Xanthopoulos, Phys. Lett. B **178**, 163 (1986).
[12] B. C. Xanthopoulos, Phys. Rev. D **34**, 3608 (1986).
[13] P. Jordan, J. Ehlers, and W. Kundt, Abh. Akad. Wiss. Mainz. Math. Naturwiss. **Kl**, 2 (1960); A. S. Kompaneets, Zh. Eksp. Teor. Fiz. **34**, 953 (1958) [Sov. Phys. JETP **7**, 659 (1958)].
[14] A. D Dagotto, R. J Gleiser, and C. O Nicasio, Classical Quantum Gravity **8**, 1185 (1991).
[15] S. Tomizawa and T. Mishima, Phys. Rev. D **90**, 044036 (2014).